Generating periodic terahertz structures in a relativistic electron beam through frequency down-conversion of optical lasers

M. Dunning, C. Hast, E. Hemsing, K. Jobe, D. McCormick, J. Nelson, T. O. Raubenheimer, K. Soong, Z. Szalata, D. Walz, S. Weathersby, and D. Xiang*

SLAC National Accelerator Laboratory, Menlo Park, California 94025, USA

(Received 5 May 2012; published 16 August 2012)

We report generation of density modulation at terahertz (THz) frequencies in a relativistic electron beam through laser modulation of the beam longitudinal phase space. We show that by modulating the energy distribution of the beam with two lasers, density modulation at the difference frequency of the two lasers can be generated after the beam passes through a chicane. In this experiment, density modulation around 10 THz was generated by down-converting the frequencies of an 800 nm laser and a 1550 nm laser. The central frequency of the density modulation can be tuned by varying the laser wavelengths, beam energy chirp, or momentum compaction of the chicane. This technique can be applied to accelerator-based light sources for generation of coherent THz radiation and marks a significant advance toward tunable narrow band THz sources.

DOI: 10.1103/PhysRevLett.109.074801 PACS numbers: 29.27.−a, 41.60.Cr, 41.75.Ht, 42.65.Ky

Generation of density modulation in relativistic electron beams with varying periods ranging from millimeters to Ångstroms is of fundamental interest in accelerator physics. An x-ray free electron laser (FEL) is an example where the electrons are packed into microbunches with equal spacing in the x-ray wavelength range from the sustained electron-radiation interaction in a long undulator [1–3]. This density modulation allows the electrons to radiate in phase which leads to orders of magnitude enhancement in the radiation power compared to the spontaneous radiation, making FELs unique in providing tunable high-power short-wavelength radiation for various areas of science [4,5].

In the optical-to-ultraviolet wavelength region, the classic way to introduce density modulation in an electron beam is through laser modulation [6–12]. In these schemes, typically a laser is first used to interact with the beam in a short undulator to generate energy modulation at the laser frequency; then the energy modulation is converted into density modulation after the beam passes through a dispersive chicane. As a result, the beam density is modulated at both the laser frequency and its harmonics. The density modulated beam can be used for driving seeded FELs to generate fully coherent radiation at high harmonic frequencies of the seed laser [8–11], for phase stable net acceleration in staged laser accelerators [12,13], and for amplifying a coherent seed in the x-ray wavelength to generate mode-locked multichromatic x-rays [14].

While the generation of density modulation at optical wavelengths through laser modulation has been extensively studied, generation of density modulation at longer wavelengths remains largely unexplored, due to the lack of high-power laser sources at THz wavelengths. To meet the increasing demands of density modulated beams at THz frequencies (e.g., density modulated electron beams and proton beams may be used to resonantly excite wakefields for advanced accelerators [15,16] and for generation of narrow band THz radiation [17,18]), various alternative methods based on advanced beam and laser manipulation techniques have been proposed and demonstrated [15–22]. Recent studies show that it is also possible to generate THz density modulation in electron beams by modulating the beam energy distribution with two optical lasers with different wavelengths [23]. This scheme is analogous to the well-known difference frequency generation technique [24] which has been widely used in the laser community for generation of narrow band THz radiation, with the relativistic electron beam being the nonlinear medium. In this Letter, we report the first observation of density modulation in an electron beam at THz frequencies generated through down-conversion of the frequencies of two lasers. Furthermore, we show that the central frequency of the density modulation can be easily tuned by varying the laser frequencies, energy chirp of the electron beam, or momentum compaction of the chicane. We anticipate that this demonstrated technique will have wide applications in many accelerator-based light sources.

The principle of generating periodic THz structure in the beam charge density by modulation with two optical lasers is rather simple [23]. For an electron beam with uniform density distribution, its longitudinal phase space distribution can be written as $f_0(p) = N_0(2\pi)^{-1/2}e^{-p^2/2}$, where N_0 is the number of electrons per unit length, $p = (E - E_0)/\sigma_E$ is the energy deviation of a particle normalized to the intrinsic beam energy spread σ_E, and E_0 is the average beam energy. After interacting with two lasers with wave numbers k_1 and k_2 in two modulators, the beam energy is modulated with the amplitude ΔE_1 and ΔE_2, and the final energy deviation p' is related to the initial deviation p by the equation $p' = p + A_1 \sin(k_1 z) + A_2 \sin(k_2 z + \phi)$, where $A_{1,2} = \Delta E_{1,2}/\sigma_E$ is

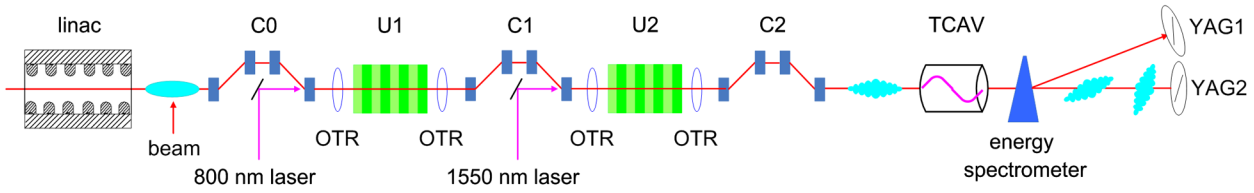

FIG. 1 (color online). Schematic layout of the beam line for generation of THz density modulation in a relativistic electron beam through laser modulation at SLAC's NLCTA [25,26].

the dimensionless energy modulation in the first and second modulator, z is the longitudinal coordinate in the beam, and ϕ is the relative phase difference between the two lasers. After further passing through a chicane with momentum compaction R_{56}, in general, the beam density distribution will consist of modulations at the wave number $k_{n,m} = nk_1 + mk_2$, where n and m are integers. It is straightforward to see that with $n = 1$ and $m = -1$ (or vice versa), a density modulation at the difference frequency of the two lasers can be generated. This allows the generation of long-scale density modulations in electron beams through short-scale energy modulations.

An experimental test of this scheme was carried out using the echo-enabled harmonic generation (EEHG) beam line [25,26] at SLAC's Next Linear Collider Test Accelerator (NLCTA). The layout of the beam line is schematically shown in Fig. 1. The electron beam with ~40 pC charge is generated in a 1.6 cell S-band (2.856 GHz rf frequency) photocathode rf gun and further accelerated to 120 MeV with two X-band (11.424 GHz rf frequency) linac structures. The main elements of the beam line consist of 3 chicanes ($C0$, $C1$, and $C2$), 2 undulators ($U1$ and $U2$), an rf transverse cavity (TCAV), quadrupoles for beam matching and focusing, and several optical transition radiation (OTR) and Yttrium Aluminum Garnet (YAG1 and YAG2) screens for measuring the position and distribution of the lasers and electron beams.

In this experiment, we aim to generate density modulation at 12 THz, corresponding to $n = -1$ and $m = 2$ for two lasers with wavelengths of 800 nm and 1550 nm. In Fig. 1, the chicane $C0$ is used to generate an orbit bump to allow laser injection into the first undulator $U1$ where the 800 nm laser (1 ps FWHM, Ti:Sapphire) interacts with the electron beam to imprint energy modulation. While chicane $C1$ is not necessary for generation of THz density modulation, it is required in the current setup for the injection of the 1550 nm laser [0.55 ps FWHM, produced by an optical parametric amplifier (OPA) system pumped with the 800 nm laser] into undulator $U2$. In this experiment, the momentum compaction of $C1$ is set at $R_{56}^{(1)} = 1.0$ mm, the minimal value required for the electron beam to bypass the laser injection mirror. While the presence of chicane $C1$ slightly changes the optimal values of the laser energy modulation for maximizing the density modulation, the underlying physics is similar to that described in the original proposal [23].

One important parameter that characterizes the density modulation is the bunching factor $b_{n,m}$, which is defined as $\langle (N(z)/N_0)e^{-izk_{n,m}} \rangle$, where the brackets denote averaging over the longitudinal coordinate z. For our experimental setup, the bunching factor is found to be,

$$b_{n,m} = |J_m[(n + Km)A_2B_2]e^{-(1/2)[nB_1+(n+Km)B_2]^2} \times J_n\{A_1[nB_1 + (n + Km)B_2]\}|, \quad (1)$$

where $J_{n,m}$ is the Bessel function of the first kind, $K = k_2/k_1$, and $B_{1,2} = R_{56}^{(1),(2)}k_1\sigma_E/E_0$ is the dimensionless momentum compaction of chicane $C1$ ($C2$).

Given the momentum compaction of $C1$ at 1 mm and that of $C2$ at the maximal value $R_{56}^{(2)} = 10.0$ mm (limited by the aperture of the vacuum pipe), the bunching factor $b_{-1,2}$ for various energy modulation amplitudes from the two lasers is calculated using Eq. (1) and shown in Fig. 2(a). The energy modulations that maximize the bunching are found to be $\Delta E_1 \approx 40$ keV and $\Delta E_2 \approx 140$ keV. In our experiment, the relatively low efficiency of the OPA and low transport efficiency limited the energy of the 1550 nm laser to ~10 μJ which limited the

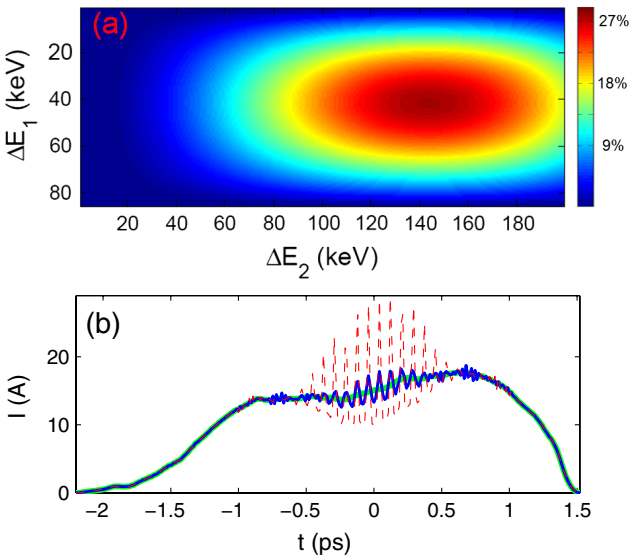

FIG. 2 (color online). (a) Electron beam THz bunching for various laser energy modulations; (b) Simulated beam density distribution for $\Delta E_2 = 50$ keV (solid blue) and $\Delta E_2 = 140$ keV (dashed red) with $\Delta E_1 = 40$ keV. The initial beam distribution without laser modulations is shown in bold green.

achievable ΔE_2. Simulation with ELEGANT code [27] using the measured beam and laser parameters indicates that noticeable density modulation at THz frequencies can still be generated with this energy modulation, as illustrated in Fig. 2(b) In this simulation, we assume $\Delta E_1 = 40$ keV. Since the laser pulse is shorter than the electron bunch, density modulation is only present for part of the beam. The simulation indicates that about 10% density modulation at 12 THz may be generated with $\Delta E_2 = 50$ keV. While the modulation depth is about a factor of 3 smaller than the optimal case at $\Delta E_2 = 140$ keV, it is sufficient to demonstrate the principle of this technique.

To generate the density modulation, the two lasers need to interact with the beam simultaneously, which requires the lasers to overlap with the electron beam both spatially and temporally in the undulators. The spatial overlap is achieved by steering the laser beam with two remote controlled mirrors to the same position as the electron beam on the OTR screens upstream and downstream of the undulators. The laser and undulator radiation generated by the electron beam is reflected out by an OTR screen downstream of each undulator and further guided to a fast photodiode for determining the rough temporal offset of the laser beam and electron beam. By referencing the signals to a fast external trigger, the laser and beam can be synchronized to within 30 ps. A delay stage is then used to finely adjust the relative timing until coherent radiation enhancement downstream of the chicane is observed. The enhancement is produced when the beam is energy modulated by the laser and further bunched by the subsequent chicane. This method has been routinely used to overlap the laser and electron beam in space and time.

After setting the delay stages such that the two lasers both interact with the electron beam, we first maximized the energy modulation from the 1550 nm laser. The energy modulation is measured at the YAG1 screen (see Fig. 1) downstream of an energy spectrometer with dispersion of 1.5 m. Three quadrupoles upstream of the spectrometer were used to provide $\beta_x \approx 0.25$ m at YAG1, where β_x is the horizontal beta function at the screen. Under this condition, the horizontal beam size at YAG1 is dominated by energy spread. The energy resolution is estimated to be approximately 10 keV.

A representative beam image measured at YAG1 with lasers off is shown in Fig. 3(a). With laser modulation, the horizontal beam size at YAG1 will increase due to the increased energy spread. In our experiment, the beam energy, laser timing, and the electron-laser spatial overlap are finely adjusted to maximize the energy modulation from the 1550 nm laser. A typical beam image at YAG1 with maximal energy modulation from the 1550 nm laser is shown in Fig. 3(b). For comparison, the energy distributions for these two cases are shown in Fig. 3(c) (the horizontal axis is converted to energy). The FWHM of the projected energy distribution approximately equals

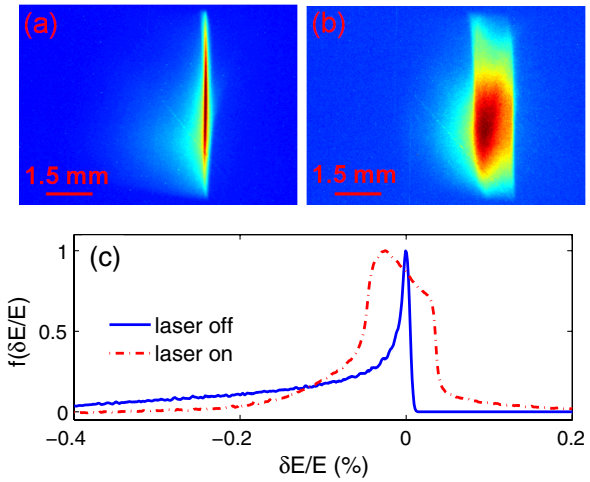

FIG. 3 (color online). Raw images of beam transverse profile measured at YAG1 with lasers off (a) and with 1550 nm laser on (b); (c) Projected beam energy distribution with lasers off (blue solid line) and with 1550 nm laser on (red dashed line).

twice the energy modulation and the maximal peak energy modulation from the 1550 nm laser is estimated to be about $\Delta E_2 = 50$ keV. Using a similar method, the power of the 800 nm laser is adjusted to provide approximately 40 keV energy modulation to maximize the density modulation, following the simulation result in Fig. 2(a).

The density modulation is measured at the YAG2 screen with a 27-cell TCAV (see Fig. 1), an rf structure operating in the TM01 mode. Its high temporal resolution and simple calibration make a TCAV well suited for the absolute measurement of beam density distributions [28–30]. When a beam passes through a TCAV at the zero-crossing phase, the TCAV imprints a vertical angular kick on the beam that varies linearly with the longitudinal position ($y' \propto t$). After about 90 degrees of phase advance in the vertical plane, the angular distribution is converted to a spatial distribution, and the vertical axis on the YAG2 screen downstream of the TCAV becomes the time axis ($y \propto t$). The absolute time measurement is calibrated by scanning the TCAV phase and recording the vertical beam centroid motion on the screen. The calibration coefficient is 170 fs/mm on the YAG2 screen. With the TCAV off, the rms beam size on the YAG2 screen is about 180 μm, corresponding to a temporal resolution of about 30 fs in this experiment.

Representative beam images measured at YAG2 with lasers off and lasers on are shown in Figs. 4(a) and 4(b), respectively. The density modulation is clearly seen in Fig. 4(b). Figure 4(c) shows the projected beam density distribution, which is in good agreement with the simulation shown in Fig. 2(b). The number of periods of the density modulation roughly equals the ratio of laser pulse width to the wavelength of the modulation; about 10 oscillations are observed in this experiment. Because the modulation bandwidth is inversely proportional to the

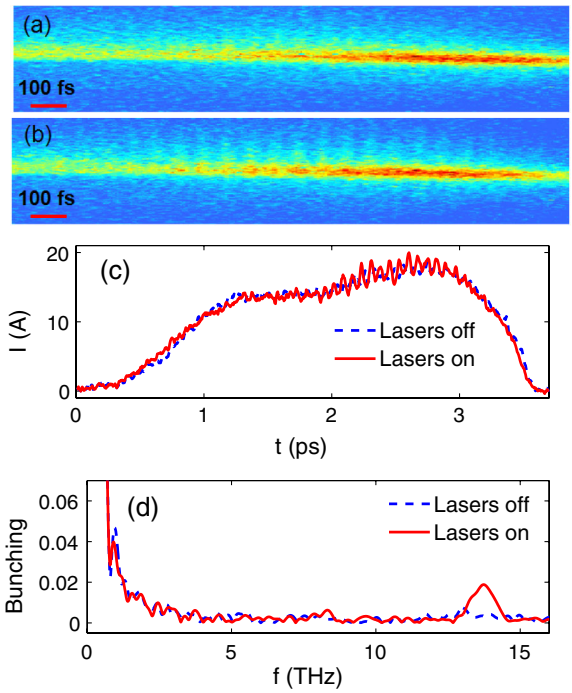

FIG. 4 (color online). Raw images of beam density distribution (only part of the beam distribution is shown for purpose of visualization) measured with TCAV with the lasers off (a) and lasers on (b); Projected beam current distribution (c) and the corresponding spectrum (d).

number of oscillations, using lasers with longer pulses will provide more oscillations which will lead to a narrower modulation bandwidth.

The bunching factor is obtained from a Fourier transformation of the beam density distribution and is shown in Fig. 4(d). From Fig. 4(d), the central frequency of the density modulation is found to be about 13.6 THz, which slightly deviates from the theoretical value of 12 THz. This discrepancy could be caused by the uncertainty of the exact wavelength of the 1550 nm laser, of which the wavelength was measured using a spectrometer with a resolution of about 5 nm. The energy chirp (correlation of energy and longitudinal position) of the beam from wakefields and the X-band linac structures may also shift the central frequency of the modulation, similar to that in the EEHG technique [25,31]. These effects could lead to a different bunching frequency from that predicted under ideal conditions. With an energy chirp h, the wave number of the density modulation will shift to,

$$k_{n,m}(h) = nC_1C_2k_1 + mC_2k_2, \tag{2}$$

where $C_1 = 1/(1 + hR_{56}^{(1)})$ is the compression factor of chicane $C1$, and $C_2 = (1 + hR_{56}^{(1)})/(1 + h(R_{56}^{(1)} + R_{56}^{(2)}))$ is the compression factor of chicane $C2$.

To identify the cause of the the frequency shift, we varied the momentum compaction of chicane $C1$, and the central frequencies of the density modulation were

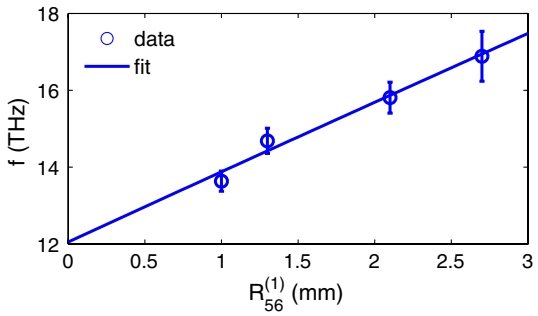

FIG. 5 (color online). Central frequency of density modulation for various momentum compactions of chicane $C1$.

recorded and shown in Fig. 5. Fitting the data to Eq. (2), the wavelength of the second laser was determined to be about 1548 nm and the beam energy chirp about 5.1 m^{-1}, corresponding to 1.2 degrees off-crest acceleration in the linac structure. This measurement also confirms that one can vary the momentum compaction of the chicane between the two modulators to change the central frequency of the density modulation in an energy chirped beam.

In fact, inclusion of a chicane between the two modulators allows the generation of THz structures in an energy chirped beam even with two lasers of the same wavelengths. This scenario can be understood as a four step process: First, the laser interacts with the beam in $U1$ and generates energy modulation at the wave number k_1. Second, the modulation is compressed (or decompressed) to C_1k_1 from the combination of energy chirp and momentum compaction of chicane $C1$. Third, the energy modulation at C_1k_1 is superimposed with the energy modulation at k_1 from the second laser in $U2$. Last, the difference frequency of the energy modulation at $(C_1 - 1)k_1$ is compressed (or decompressed) again with compression factor C_2, and is further converted into density modulation at $(C_1 - 1)k_1C_2$ after passing through chicane $C2$. This configuration may greatly extend the applicability of the original proposal [23] and will make narrow band THz radiation accessible to more facilities.

In summary, we have presented the first observation of density modulation at THz frequencies in a relativistic electron beam through down-conversion of the energy modulations from two lasers. One of the many advantages of the demonstrated technique is the flexibility it offers to tune the central frequency of the modulation, which can be achieved through tuning of laser wavelengths, beam energy chirp, or chicane momentum compaction. In principle, this allows one to generate density modulation in the beam covering the whole THz range. Once the density modulation is formed, it is straightforward to use the beam for generation of coherent narrow band THz radiation. Future plans at NLCTA are to upgrade the OPA, which will increase the energy modulation from the second laser, thereby, increasing the depth of the density modulation. The beam with strong density modulation will then be used

to generate intense narrow band THz radiation which will be characterized with a Michelson interferometer and a cryogenically cooled bolometer.

We thank F. Wang for help in operating the transverse cavity. This work was supported by the US DOE Office of Basic Energy Sciences using the NLCTA facility which is partly supported by the US DOE Office of High Energy Physics under Contract No. DE-AC02-76SF00515.

*dxiang@slac.stanford.edu

[1] W. Ackermann *et al.*, Nature Photon. **1**, 336 (2007).
[2] P. Emma *et al.*, Nature Photon. **4**, 641 (2010).
[3] D. Pile, Nature Photon. **5**, 456 (2011).
[4] Z. Huang and K.-J. Kim, Phys. Rev. ST Accel. Beams **10**, 034801 (2007).
[5] B. W. J. McNeil and N. R. Thompson, Nature Photon. **4**, 814 (2010).
[6] B. Girard, Y. Lapierre, J. M. Ortega, C. Bazin, M. Billardon, P. Elleaume, M. Bergher, M. Velghe, and Y. Petroff, Phys. Rev. Lett. **53**, 2405 (1984).
[7] G. De Ninno *et al.*, Phys. Rev. Lett. **101**, 053902 (2008).
[8] L.-H. Yu, Phys. Rev. A **44**, 5178 (1991).
[9] L.-H. Yu *et al.*, Phys. Rev. Lett. **91**, 074801 (2003).
[10] G. Stupakov, Phys. Rev. Lett. **102**, 074801 (2009).
[11] D. Xiang and G. Stupakov, Phys. Rev. ST Accel. Beams **12**, 030702 (2009).
[12] C. Sears *et al.*, Phys. Rev. ST Accel. Beams **11**, 101301 (2008).
[13] W. Kimura *et al.*, Phys. Rev. Lett. **86**, 4041 (2001).
[14] D. Xiang, Y. Ding, T. Raubenheimer, and J. Wu, Phys. Rev. ST Accel. Beams **15**, 050707 (2012).
[15] P. Muggli, V. Yakimenko, M. Babzien, E. Kallos, and K. P. Kusche, Phys. Rev. Lett. **101**, 054801 (2008).
[16] N. Kumar, A. Pukhov, and K. Lotov, Phys. Rev. Lett. **104**, 255003 (2010).
[17] S. Bielawski *et al.*, Nature Phys. **4**, 390 (2008).
[18] Y. Shen, X. Yang, G. L. Carr, Y. Hidaka, J. B. Murphy, and X. Wang, Phys. Rev. Lett. **107**, 204801 (2011).
[19] Y.-E Sun, P. Piot, A. Johnson, A. H. Lumpkin, T. J. Maxwell, J. Ruan, and R. Thurman-Keup, Phys. Rev. Lett. **105**, 234801 (2010).
[20] P. Piot, Y.-E. Sun, J. G. Power, and M. Rihaoui, Phys. Rev. ST Accel. Beams **14**, 022801 (2011).
[21] D. Xiang and A. Chao, Phys. Rev. ST Accel. Beams **14**, 114001 (2011).
[22] P. Musumeci, R. K. Li, and A. Marinelli, Phys. Rev. Lett. **106**, 184801 (2011).
[23] D. Xiang and G. Stupakov, Phys. Rev. ST Accel. Beams **12**, 080701 (2009).
[24] Robert W. Boyd, *Nonlinear Optics* (Academic Press, New York, 2003), 2nd ed.
[25] D. Xiang *et al.*, Phys. Rev. Lett. **105**, 114801 (2010).
[26] D. Xiang *et al.*, Phys. Rev. Lett. **108**, 024802 (2012).
[27] M. Borland, Advanced Photon Source LS-287, September (2000).
[28] G. Berden *et al.*, Phys. Rev. Lett. **99**, 164801 (2007).
[29] K. Bane *et al.*, Phys. Rev. ST Accel. Beams **12**, 030704 (2009).
[30] D. Xiang *et al.*, Phys. Rev. ST Accel. Beams **14**, 112801 (2011).
[31] Z. Huang, D. Ratner, G. Stupakov, and D. Xiang, in *Proceedings of FEL 09* (Liverpool, 2009), p. 127.